Monte Carlo study of dc and ac vertical electron transport in a single-barrier heterostructure

A. Reklaitis
Semiconductor Physics Institute, Goštauto 11, 2600 Vilnius, Lithuania

G. Grigaliūnaitė
Gediminas Technical University, Saulėtekio aleja 11, 2040 Vilnius, Lithuania

(Received 8 May 2000; published 23 March 2001)

Steady-state dc and large-signal ac vertical electron transport in a single barrier $In_{0.53}Ga_{0.47}As/AlAs/In_{0.53}Ga_{0.47}As$ structure is investigated by ensemble Monte Carlo simulations self-consistently coupled with the Poisson equation. The comparison of the calculated steady-state current-voltage characteristic with the experimental data indicates the strong influence of Γ-X-Γ resonant tunneling on the dc current-voltage characteristic of the $In_{0.53}Ga_{0.47}As/AlAs/In_{0.53}Ga_{0.47}As$ structure. The Monte Carlo technique is applied for an evaluation of the capacitance-voltage characteristic of this structure. The calculated capacitance-voltage characteristic is compared with the corresponding experimental results. Frequency-dependent harmonic amplitudes are also evaluated from the calculated large-signal ac response.

DOI: 10.1103/PhysRevB.63.155301 PACS number(s): 73.40.Kp, 72.20.−i, 72.30.+q, 73.40.Gk

I. INTRODUCTION

The vertical transport of charge carriers in semiconductor heterostructures has attracted much interest over the past years.[1–8] Investigations of vertical transport in heterostructures is of great importance for understanding the physical processes occurring in various advanced semiconductor structures. The most appropriate method for a theoretical study of nonequilibrium carrier transport in semiconductor structures is the ensemble Monte Carlo method. Since the pioneering work of Lebwohl and Price,[9] ensemble Monte Carlo simulations, self-consistently coupled with the Poisson equation, have been widely used for the calculation of the current-voltage (I-V) characteristic of various semiconductor structures and devices. In this study, steady-state dc and large-signal ac vertical electron transport in a single-barrier heterostructure is investigated using the Monte Carlo method.

Parallel with the I-V characteristic, the capacitance-voltage (C-V) relationship is the fundamental characteristic of any structure. The capacitance is often estimated from a change of the space charge ΔQ in a certain region of the structure, such change being induced by a change of the corresponding bias voltage ΔV. Such a method for the evaluation of the C-V characteristic is complicated, however, and care must be used to define the domain over which the change of the space charge is specified. In this study, a direct Monte Carlo method is applied for a calculation of the C-V characteristic of a single-barrier heterostructure.

II. MODEL

Single-barrier heterostructures are devices used for the efficient frequency multiplication of microwave radiation into the submillimeter frequency range.[10–13] Experimental investigations[14] of a single-barrier structure designed from $In_{0.53}Ga_{0.47}As/AlAs/In_{0.53}Ga_{0.47}As$ heterojunctions indicated that it has an excellent capacitance modulation characteristic for frequency multiplication. Therefore, the $In_{0.53}Ga_{0.47}As/AlAs/In_{0.53}Ga_{0.47}As$ structure was chosen for a comparison of the present Monte Carlo simulations with the experimental results set out in Ref. 14.

The simulated structure corresponds to that experimentally studied.[14] It consists of five layers: (1) $In_{0.53}Ga_{0.47}As$ (300 nm, $N_d = 1.2\times10^{17}$ cm^{-3}); (2) undoped $In_{0.53}Ga_{0.47}As$ (5 nm); (3) AlAs (5 nm); (4) a repeat of (2); and finally, (5) a repeat of (1). The heavily doped contact layers of the experimentally investigated structure[14] are replaced in the simulations by thermally injecting contacts with the corresponding electron density 2.2×10^{19} cm^{-3}. It is assumed that the electrons are in thermal equilibrium with the lattice in the contacts. The electrons are injected from both contacts with the equilibrium Maxwellian distribution. The probability distribution of the random wave vector components, normal to the contact surface k_z and the parallel components k_x and k_y of the injected electron, is given by

$$P(k_x,k_y,k_z) = A\,\nu_z(\mathbf{k})\times\exp[-E(\mathbf{k})/2k_BT], \quad k_z>0, \tag{1}$$

where A is the normalizing constant, ν_z is the normal to the contact surface velocity component, E is the electron kinetic energy, k_B is the Boltzmann constant, and T is the lattice temperature. Electron injection is taken into account both from the cathode and the anode. The average rate of electron injection from the contact is expressed as

$$\Gamma = \overline{\frac{dN}{dt}} = Sn^+\sqrt{\frac{k_BT}{2\pi m}}, \tag{2}$$

where S is the cross-section area of the structure, n^+ is the electron concentration in the contact, and m is the electron effective mass. The injection event of each individual electron is independent of the injection events of the other electrons. Therefore, the injection process is a stochastic Poissonian process. The number of injected electrons N during time step Δt obeys the Poissonian distribution

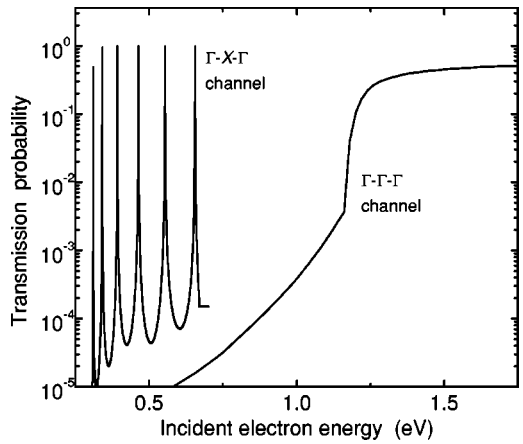

FIG. 1. The transmission probability of electron tunneling through an $In_{0.53}Ga_{0.47}As/AlAs/In_{0.53}Ga_{0.47}As$ barrier of 50-nm thickness as a function of incident energy. The transmission probability via the Γ-Γ-Γ channel was obtained from Eq. (A5) of the present study for an electric field in the barrier $F=100$ kV/cm. The transmission probability via the Γ-*X*-Γ channel was calculated from Eq. (15) of Ref. 26. The results were obtained for the wave-vector component parallel to heterointerface $k_{II}=0$.

$$P_N(\Delta t)=\frac{(\Gamma\Delta t)}{N!}\exp(-\Gamma\Delta t). \tag{3}$$

Probability distribution (3) is taken into consideration for a simulation of temporal electron injection. The number N of electrons injected from each contact during each time step Δt is chosen randomly in accordance with Eq. (3). The components of the wave vector of each injected electron are selected as random quantities, which satisfy the probability distribution given by Eq. (1).

We have also considered the injection process, taking into account a Fermi-Dirac distribution of thermally equilibrium electrons in the contacts. In this case, the electron injection rate is changed to

$$\Gamma=\frac{\overline{dN}}{dt}=Sn^{+}\sqrt{\frac{k_BT}{8m}}\frac{\Phi_1(E_F/k_BT)}{\Phi_{1/2}(E_F/k_BT)}, \tag{4}$$

where Φ_1 and $\Phi_{1/2}$ are the Fermi integrals of order 1 and 1/2, respectively, and E_F is the energy of the Fermi level. The value $E_F=0.6175$ eV is obtained from a numerical solution of the equation $n^{+}=2[2\pi mk_BT/(2\pi\hbar)^2]^{3/2}\Phi_{1/2}(E_F/k_BT)$. The probability distribution of the random wave-vector components of injected electrons is also changed, taking into account the Fermi-Dirac statistics. The calculations of *I*-*V*, *C*-*V*, relationships and ac response of the single-barrier structure are performed for both models of carrier injection. It is found that the difference between the results obtained by using Maxwell-Boltzmann and Fermi-Dirac statistics of carrier injection does not exceed 1–2 %.

The energy-band structure of the materials composing the structure includes Γ, *L*, and *X* nonparabolic valleys. Polar optical, deformation acoustic, ionized impurity, and all intervalley scattering processes are considered. The material parameters for $In_{0.53}Ga_{0.47}As$ and for AlAs are taken from Refs. 15 and 16, respectively. The band offset between the Γ valleys of AlAs and $In_{0.53}Ga_{0.47}As$ is accepted as 1.2 eV (Refs. 17 and 18). The self-consistent potential distribution is derived from the solution of the Poisson equation at each time step. A small time step of 1-fs duration was chosen in order to avoid the numerical instabilities. The Poisson equation was solved on a uniform spatial mesh with 1000 nodes. The calculations were carried out for 100 000 simulated particles.

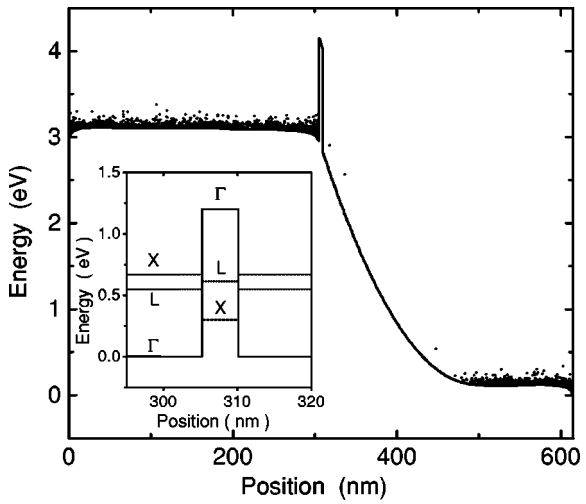

FIG. 2. Potential profile, i.e., Γ valley edge (solid curve) and distribution of electron kinetic energy (points) for a bias voltage of 3 V. The inset shows the energy-band diagram of the structure.

Heterojunctions were treated as abrupt interfaces. Electron tunneling and thermionic emission through the heterointerfaces was taken into account. The triangular and trapezoidal shapes of the potential barriers were considered for electron tunneling according to the energy of the impinging electron: trapezoidal for the low-energy values and triangular for the high-energy values, respectively. The transmission probability for tunneling through the triangular barrier,[19] which takes into account the electron effective mass discontinuity at the heterointerfaces, was used in the present calculations.

Most electrons tunnel through the trapezoidal barrier due to the large Γ-Γ band offset between the Γ valleys of the considered structure. The transmission probability through the trapezoidal barrier via the Γ-Γ-Γ channel was derived by solving the Schrödinger equation, and by taking into account the discontinuity of the effective mass at the heterointerfaces (see the Appendix).

As is seen from the energy-band diagram presented in the insert of Fig. 2, resonant tunneling via the Γ-*X*-Γ channel[20–25] may play a significant part in the tunneling process through the AlAs barrier in the $In_{0.53}Ga_{0.47}As/AlAs/In_{0.53}Ga_{0.47}As$ structure. In the present study, the tunneling through the Γ-*X*-Γ channel is taken into account by assuming a rectangular potential barrier, and by using the Γ-*X*-Γ transmission probability derived in Ref. 26. The assumption of a rectangular barrier is reasonable, because the energy range over which the bound states exist in AlAs layer is between $E_2>E>E_1$, where $E_1=E_{\Gamma\Gamma}-E_{\Gamma X(\mathrm{AlAs})}=0.3$ eV, and $E_2=E_{\Gamma X(\mathrm{In}_x\mathrm{Ga}_{1-x}\mathrm{As})}=0.67$ eV.

Thus, the electron can suffer resonant Γ-X-Γ tunneling in an energy range essentially below the Γ-Γ band offset $E_{\Gamma\Gamma}=1.2$ eV. The value of the adjustable parameter t (Ref. 26), which represents the extent of the Γ-X mixing in the Γ-X-Γ tunneling, is estimated from a comparison of the calculated and experimental I-V characteristics of the structure. The dependence of the transmission probability on the incident electron energy is shown in Fig. 1.

These transmission probabilities were then used in the Monte Carlo simulations according to the energy of the impinging electron. Both tunneling channels, Γ-Γ-Γ and Γ-X-Γ, were taken into account for the electron energy range between 0.3 and 0.67 eV (see Fig. 2). Tunneling via the Γ-Γ-Γ channel was only considered for the electron energy outside this range. The shape of the potential barrier was updated each time step from the solution of the Poisson equation. The transmission probabilities for the Γ-Γ-Γ and Γ-X-Γ channels were calculated for each electron impinging the barrier. The tunneling process was then treated in the Monte Carlo simulation as a scattering event. A random number r, uniformly distributed between 0 and 1, was generated. The electron was allowed to tunnel if the inequality $D<r$ was satisfied. Otherwise, the electron was reflected from the barrier, i.e., its wave vector component k_z, normal to the heterointerface was changed to $-k_z$.

III. *I*-*V* CHARACTERISTIC

The steady-state potential profile and electron distribution in the $In_{0.53}Ga_{0.47}As/AlAs/In_{0.53}Ga_{0.47}As$ structure are presented in Fig. 2. The majority of electrons are located in the $In_xGa_{1-x}As$ layer adjacent to the emitter. The electric field is low in this layer. Therefore, all electrons are distributed in the lowest Γ valley of the conduction band of this layer. The tunneling current through the AlAs barrier is dominant for the bias voltages below 10 V. A thermionic current over the barrier was not observed in this range of bias voltage.

For the ensemble Monte Carlo simulations, the current density j is usually evaluated in accordance with Shockley-Ramo theorem as[27]

$$j=\frac{\sigma}{L}\sum_{i=1}^{N}\nu_z(\mathbf{k}_i), \tag{5}$$

where σ is the particle charge per unit area, L is the length of the structure, N is the number of simulated particles, ν_z is the velocity of the particle in the z direction, and $\mathbf{k}_i$ is the wave vector of the ith particle. Serious difficulties exist, however, in the evaluation of the steady-state current from Eq. (5) when electron tunneling controls the current. The level of the fluctuations in the current density obtained from the Monte Carlo simulations may essentially exceed the exact value j_0, even though an extremely large number of particles are simulated. Such a situation occurs when the average transmission probability of the electron tunneling is below unity by several orders of magnitude. In such a case, most of the particles impinging on the barrier are reflected, and only a few of them are tunneling and making a contribution to the current. Due to this, Eq. (5) is not appropriate for an evaluation of the steady state current for structures in which the tunneling current is predominant. This is evident from the following considerations:

The accuracy of the current density evaluated from the Monte Carlo simulations by using Eq. (5) can be estimated as follows: Assume for simplicity that the intercarrier interaction is negligible, and that electrons are moving in a self-consistent and non-fluctuating electric field. Let us also neglect the fluctuations in a number of simulated particles, which are caused by random particle injection from the contacts. Under these conditions the statistical fluctuations of the calculated current density can be estimated by introducing the momentum distribution function

$$F(\mathbf{k})=\frac{\int_0^L f(\mathbf{k},z)\,dz}{\int_0^L\int f(\mathbf{k},z)\,d\mathbf{k}dz}, \tag{6}$$

normalized to unity, where $f(\mathbf{k},z)$ is the electron distribution function normalized to the local electron concentration $n(z)$. The distribution function $F(\mathbf{k})$ corresponds to the momentum distribution of all the electrons in the structure. The variance var(j) of the calculated current density j, i.e., the mean value of the square of current fluctuations $\langle\delta j^2\rangle$, can be obtained from Eq. (15) of Ref. 28. The resulting expression for the variance var(j) of the calculated current density is given by

$$\frac{\langle\delta j\rangle^2}{j_0^2}=\frac{1}{N}\left\{\frac{\int\nu_z^2(\mathbf{k})F(\mathbf{k})d\mathbf{k}}{\left[\int\nu_z(\mathbf{k})F(\mathbf{k})d\mathbf{k}\right]^2}-1\right\}, \tag{7}$$

where j_0 is the exact value of the current density, and N is the number of simulated particles. Equation (7) is valid for the estimation of the accuracy of Monte Carlo simulations for any two terminal structures.

In a case where the tunneling current is dominant over the thermionic one, most of the electrons are accumulated in the region where the electric field is low, as seen from Fig. 2. The electrons are in a state close to the thermal equilibrium in this region. Assuming that the electrons are in thermal equilibrium in the whole structure (the high-field region on the collector side of the structure is depleted of electrons; see Fig. 2), from Eq. (7) we obtain the variance $\langle\delta j^2\rangle$ of the calculated current density. The result is given by

$$\frac{\langle\delta j^2\rangle}{j_0^2}=\frac{1}{N}\frac{\langle\nu_{th}^2\rangle-\langle\nu_d\rangle^2}{\langle\nu_d\rangle^2}, \tag{8}$$

where $\langle\nu_{th}^2\rangle$ is the squared mean velocity of all the electrons, and $\langle\nu_d\rangle$ is the electron drift velocity averaged over the whole structure. In accordance with Eq. (8), an extremely large number of particles should be simulated in order to obtain a reasonably accurate calculated current density when the transmission probability of the electron tunneling D is significantly less than unity. For example, assume that the transmission probability is $D=10^{-4}$ for the electrons at ther-

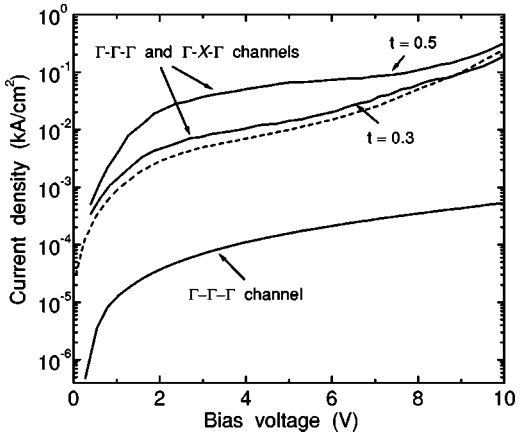

FIG. 3. Comparison of the calculated steady state *I*-*V* characteristic (solid curves) with the experimental results (Ref. 14) (dashed curve). The calculations were carried out considering only the Γ-Γ-Γ tunneling channel and considering both the Γ-Γ-Γ and Γ-*X*-Γ tunneling channels for two values of Γ-*X* mixing parameters $t=0.5$ and 0.3.

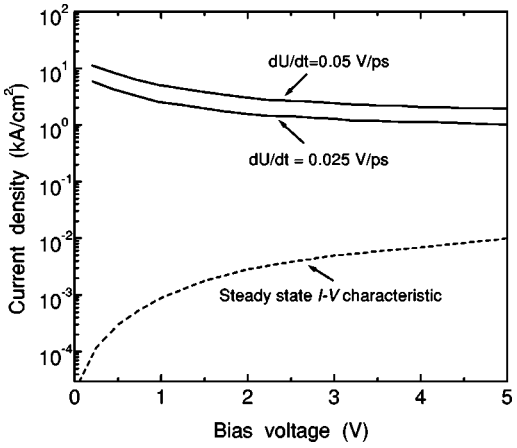

FIG. 4. Calculated current response (solid curves) to the ramp of the bias voltage. The calculations were carried for two rates $dU/dt=0.025$ and 0.05 V/ps of the increase in the bias voltage. The voltage was linearly increased from 0 to 5 V. The dashed curve shows the steady-state *I*-*V* characteristic.

mal equilibrium (Fig. 1). The average drift velocity can be estimated as $\langle \nu_d \rangle = \nu_{th} D$. From Eq. (8) we obtain that $\langle \delta j^2 \rangle / j_0^2 = (ND)^{-1}$; i.e., in order to achieve an accuracy of 10% for the calculated current, the required number of simulated particles is $N=10^8$.

This problem can be resolved by using an alternative estimator for the evaluation of the steady state current. Consider the ith Monte Carlo particle incident on a barrier. The charge per unit area of the particle is σ. The transmission probability D of the particle is dependent on its wave vector $\mathbf{k}_i$. For this particle, the fraction of the tunneling charge is $\sigma D(\mathbf{k}_i)$. By collecting all the particles impinging the barrier from the left and the right during the time step Δt, we obtain the current density, which is given by

$$j = \frac{\sigma}{\Delta t} \sum_{i=1}^{M^+} D(\mathbf{k}_i) - \frac{\sigma}{\Delta t} \sum_{j=1}^{M^-} D(\mathbf{k}_j), \tag{9}$$

where M^+ and M^- are the numbers of particles impinging on the barrier from the left and right, respectively, during the time step Δt. The accuracy of the current density obtained from Eq. (9) can be evaluated as follows. Consider a stream of Monte Carlo particles incident on a barrier from the left. The stream is a stochastic Poissonian process.[8] Assume, for simplicity, that the transmission probability is constant, i.e., independent of the energy of the incident electron. The resulting current fluctuations are caused by the Poissonian temporal fluctuations in the number of particles impinging the barrier. The variance of the calculated current density is given by

$$\langle \delta j^2 \rangle = \left(\frac{\sigma D}{\Delta t} \right)^2 \langle \delta M^{+2} \rangle = \left(\frac{\sigma D}{\Delta t} \right)^2 M^+. \tag{10}$$

Thus the accuracy of the calculated current can be estimated as

$$\frac{\langle \delta j^2 \rangle}{j_0^2} = \frac{1}{M^+}. \tag{11}$$

The value of the current fluctuations $\langle \delta j^2 \rangle$ given by Eq. (11) is lower by several orders than the corresponding value obtained from Eq. (8). It should be noted that Eq. (9) is valid only for the calculation of current under steady-state conditions. The current should be evaluated from Eq. (5) when the electron distribution is time dependent.

A comparison of the calculated steady-state *I*-*V* characteristic of the $In_{0.53}Ga_{0.47}As/AlAs/In_{0.53}Ga_{0.47}As$ structure with the experimental results[14] is shown in Fig. 3. The calculated *I*-*V* characteristic is approximately two orders below the experimental results when only tunneling via the Γ-Γ-Γ channel is considered, and the Γ-*X*-Γ channel is disregarded. The *I*-*V* characteristic obtained taking into account the Γ-Γ-Γ and Γ-*X*-Γ channels for the value of Γ-*X* mixing $t=0.5$ ($t=0.5$ was accepted in Ref. 26 for the GaAs/AlAs/GaAs heterostructure) overestimates the experimental results. The best agreement of the calculated *I*-*V* characteristic of the $In_{0.53}Ga_{0.47}As/AlAs/In_{0.53}Ga_{0.47}As$ structure with the experimental data[14] is obtained for $t=0.3$ (Fig. 3).

IV. *C*-*V* CHARACTERISTIC

The *C*-*V* characteristic of the structure is evaluated directly from the simulated current response to the linearly increasing bias voltage. The response of the current density $j(t)$ to the slowly varying bias voltage $U(t)$ can be expressed as

$$j(t) = j_0(U) + C(U) \frac{dU}{dt}, \tag{12}$$

where $j_0(U)$ is the steady-state current density for bias voltage U, and $C(U)$ is the capacitance per unit area caused by the displacement of the space charge in the structure. Once

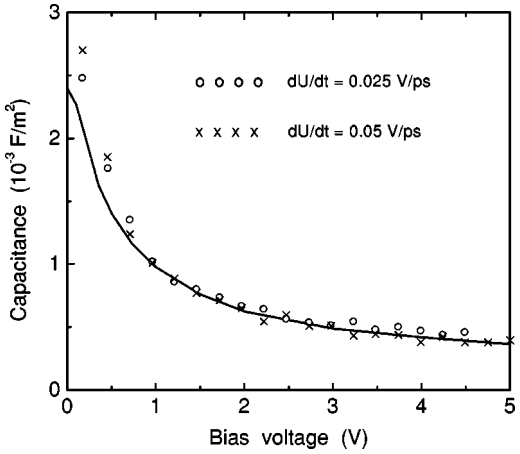

FIG. 5. *C-V* characteristic (circles and crosses) of the structure obtained from the current response presented in the Fig. 4. The solid curve shows experimental results of Ref. 14.

the steady-state *I-V* characteristic $j_0(U)$ is calculated, the current response to the linearly increasing bias voltage is simulated. The current density is estimated from Eq. (5), which is valid for the steady state as well as for time dependent transport. The *C-V* characteristic is evaluated from Eq. (12). The rate dU/dt of the bias voltage increase should be taken as sufficiently small in order to ensure stationary electron distribution in real and momentum space during the simulation of the current response.

The current response to the linearly increasing bias voltage from $U=0$ to $U=5$ V is shown in Fig. 4. The current response is calculated for two different rates dU/dt of voltage increase. It was obtained that the current response is linearly proportional to the rate dU/dt. As seen from Fig. 4, the displacement current significantly exceeds the steady-state current density j_0. Hence the steady-state current can be neglected in an evaluation of the capacitance of the structure. Figure 5 shows the *C-V* characteristic obtained from the results presented in Fig. 4. As seen from Fig. 5, the calculated *C-V* characteristic is in very good agreement with the experimental data.[14]

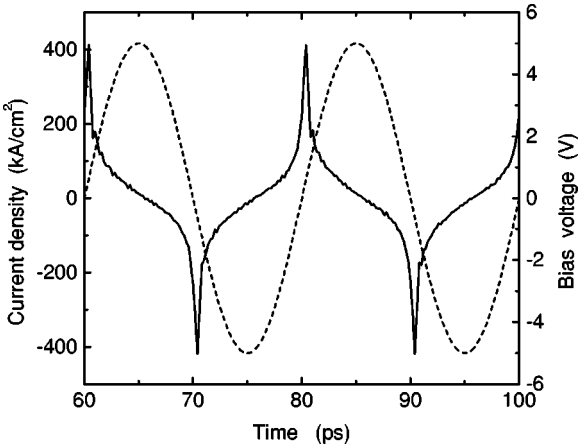

FIG. 6. Current response (solid curve) to the sinusoidal excitation of 50-GHz frequency and 5-V amplitude (dashed curve).

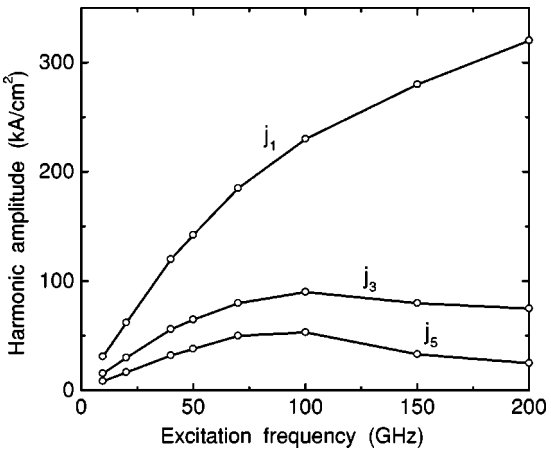

FIG. 7. First- (j_1), third- (j_3), and fifth- (j_5) harmonic amplitudes of the current response vs the excitation frequency. The amplitude of the sinusoidal excitation is 5 V.

V. LARGE-SIGNAL AC RESPONSE

The large-signal ac current response was calculated for the evaluation of the efficiency of the structure for frequency multiplication. The current response to a 50-GHz sinusoidal bias voltage is presented in Fig. 6. Odd harmonics are only generated during the frequency multiplication because of the even symmetry of the *C-V* characteristic of the symmetrical single-barrier structure. The amplitudes of the first, third, and fifth harmonics (Fig. 7) were obtained from the Fourier transform of the large-signal ac response of the current.

The current response to sinusoidal excitation is determined by the steady state *C-V* characteristic at low excitation frequencies below 50 GHz. In this frequency range, the harmonic amplitudes are linearly proportional to the excitation frequency f (Fig. 7). The response of the electron distribution in real and momentum space is stationary in this frequency range; i.e., the electron distribution is close to a

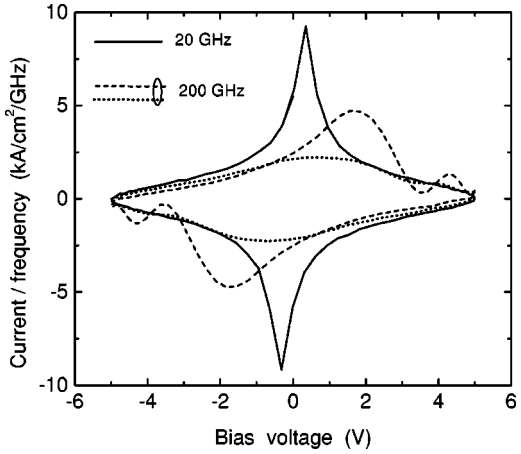

FIG. 8. Current-voltage phase portraits for the 20- (solid curve) and 200-GHz (dashed and dotted curves) sinusoidal excitation frequencies. The amplitude of the excitation is $U_0=5$ V. The current density is normalized to the excitation frequency. The dashed curve is obtained when neglecting the *X* and *L* valleys, the dotted curve is obtained when including the *X* and *L* valleys.

steady state during the ac period. At a low excitation frequency, the amplitude of the nth harmonic is defined as

$$j_n = 2\pi f U_0 \int_0^{2\pi} C(U_0 \sin\omega)\cos\omega\cos n\omega d\omega, \qquad (13)$$

where $C(U_0 \sin\omega)$ is the steady state C-V characteristic of the structure.

The efficiency of the frequency multiplication is reduced at excitation frequencies above 50 GHz, as is evident from the results presented in Fig. 7. The inertia of the electron redistribution in real and momentum space is responsible for the reduction of the efficiency at high excitation frequencies. This is evident from the j-U phase portraits presented in Fig. 8. As seen from Fig. 8, the current is determined by the steady-state C-V characteristic at an excitation frequency of 20 GHz. Contrary to this, the shape of the current response is substantially different from the one determined by the steady-state C-V characteristic at an excitation frequency of 200 GHz.

The processes responsible for the deviation of the high-frequency current response from the low-frequency response can be understood from the electron and potential distributions presented in Fig. 9. At low excitation frequencies, the distribution of the electron concentration in the structure corresponds to the steady-state distribution during the ac period [Fig. 9(a)]. At high excitation frequencies, as seen from a comparison of the electron distributions presented in Figs. 9(a) and 9(b), the electrons have no time to completely compensate for the space charge in the regions near the barrier. Due to this, the effective capacitance of the structure is significantly reduced. As a consequence, the peak value of the current is essentially lowered, as seen from Fig. 8.

At a high excitation frequency, the electrons are essentially heated in the Γ valley of the $In_xGa_{1-x}As$ layers when the upper L and X valleys are disregarded [Fig. 9(b)]. As a result, the Γ valley electrons in the $In_xGa_{1-x}As$ layers are transferred to the upper L and X valleys when intervalley scattering is taken into account [Fig. 9(c)]. This intervalley transfer essentially reduces the electron drift velocity in the $In_xGa_{1-x}As$ layers. Moreover, the electrons, which occupy the L and X valleys in the $In_xGa_{1-x}As$ layer, may surmount the $In_xGa_{1-x}As$/AlAs heterointerface thermionically, as is evident from the energy band diagram shown in the inset of Fig. 2. After the emission of optical phonons, the electrons in the X valleys of the AlAs layer are cooled and confined in the barrier [Fig. 9(c)]. The cooled electrons are able to leave the AlAs barrier only by means of tunneling. As a result, a significant space charge is accumulated in the barrier. This accumulated space charge causes an addition reduction in the peak value of the current, as seen from Fig. 8.

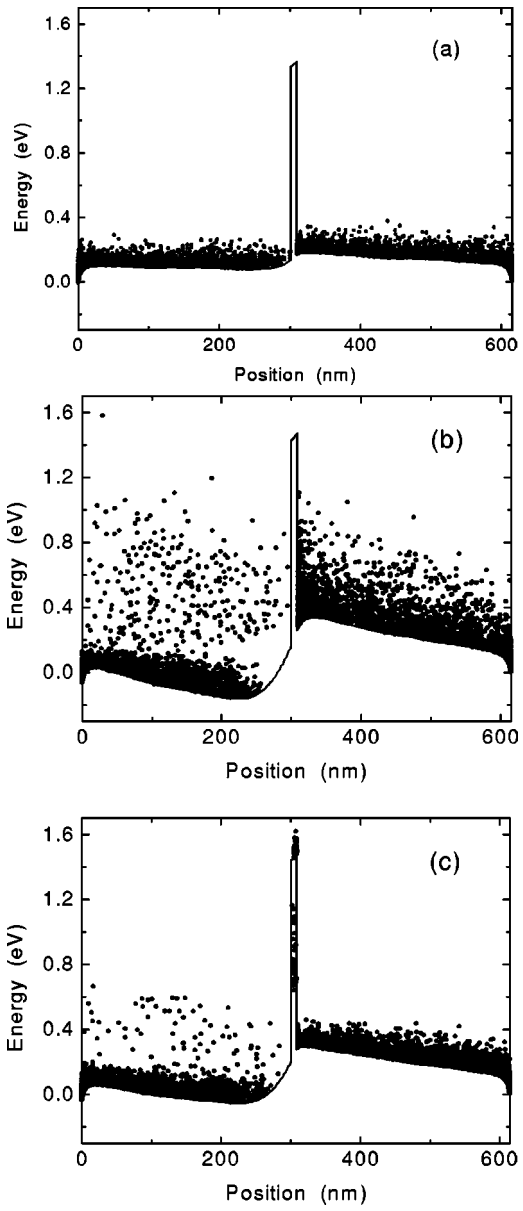

FIG. 9. Potential profile (solid curves) and distribution of electron kinetic energy (points) at the time $t=10/f$ for and ac bias voltage $U(t)=U_0\sin(2\pi ft)$, $U_0=5$ V. (a) $f=20$ GHz. (b) $f=200$ GHz, and L and X valleys are disregarded. (c) $f=200$ GHz, and L and X valleys are considered.

VI. CONCLUSIONS

Steady-state dc and time-dependent large signal ac electron transport in a single-barrier structure was investigated by Monte Carlo simulations. A comparison of the calculated I-V characteristic of the structure with the experimental data indicates that resonant Γ-X-Γ channel is the dominant tunneling mechanism of the dc transport in the $In_{0.53}Ga_{0.47}As/AlAs/In_{0.53}Ga_{0.47}As$ heterostructure. The capacitance-voltage characteristic of the structure was obtained from direct Monte Carlo simulations. The efficiency of microwave frequency multiplication by a single-barrier structure was investigated.

ACKNOWLEDGMENTS

This work was supported by the Lithuanian State Science and Studies Foundation.

APPENDIX

The three layers composing the potential barrier were characterized by indexes 1 (layer of incident electron), 2 (barrier layer), and 3 (the final layer after tunneling). The following matching conditions for the electron wave function $\psi(z)$ at the heterointerfaces were used:

$$\psi_1(0)=\psi_2(0), \tag{A1}$$

$$\frac{1}{m_1}\frac{d\psi_1(0)}{dz}=\frac{1}{m_2}\frac{d\psi_2(0)}{dz}, \tag{A2}$$

$$\psi_2(d)=\psi_3(d), \tag{A3}$$

$$\frac{1}{m_2}\frac{d\psi_2(d)}{dz}=\frac{1}{m_3}\frac{d\psi_3(d)}{dz}, \tag{A4}$$

where d is the barrier width; and m_1, m_2, and m_3 are the effective masses in the initial layer, the barrier and the final layer, respectively. The obtained transmission probability for a trapezoidal barrier is given by

$$D=\frac{4m_1k_{3z}}{\pi^2m_3k_{1z}}\frac{1}{Q^2}, \tag{A5}$$

where k_{1z} and k_{3z} are the transverse to the heterointerface wave-vector components, the incident component, and the final component, respectively:

$$\begin{aligned}Q^2=&\left\{[A_i(\eta_0)B_i'(\eta_d)-A_i'(\eta_d)B_i(\eta_0)]\right.\\&\left.+\frac{m_1k_{3z}}{m_3k_{1z}}[A_i(\eta_d)B_i'(\eta_0)-A_i'(\eta_0)B_i(\eta_d)]\right\}^2\\&+\left\{\frac{m_1k_F}{m_2k_{1z}}[A_i'(\eta_0)B_i'(\eta_\alpha)-A_i'(\eta_d)B_i'(\eta_0)]\right.\\&\left.+\frac{m_2k_{3z}}{m_3k_F}[A_i(\eta_0)B_i(\eta_d)-A_i(\eta_d)B_i(\eta_0)]\right\}^2.\end{aligned} \tag{A6}$$

A_i and B_i are Airy functions, and A_i' and B_i' are their derivatives:

$$k_F=(2m_2eF/\hbar^2)^{1/3}, \tag{A7}$$

$$\eta_0=k_F(U_0-E_{2z})/eF, \tag{A8}$$

$$\eta_d=k_F(U_0-E_{2z}-eFd)/eFd, \tag{A9}$$

$$E_{2z}=E_1-\hbar^2k_{II}^2/2m_2. \tag{A10}$$

e is the electron charge, $\hbar$ is the Planck constant, U_0 is the barrier height, F is the electric-field strength in the barrier, d is the barrier width, E_1 is the energy of the incident carrier, and k_{II} is the wave-vector component parallel to the heterointerface.

[1] F. Chevoir and B. Vinter, Phys. Rev. B **47**, 7260 (1993).
[2] M. Morifuji and C. Hamaguchi, Phys. Rev. B **52**, 14 131 (1995).
[3] Y.X. Liu, D.Z.-Y. Ting, and T.C. McGill, Phys. Rev. B **54**, 5675 (1996).
[4] L.P. Fu, F.T. Bacalzo, G.D. Gilliland, R. Chen, K.K. Bajaj, and J. Klem, Phys. Rev. B **51**, 17 630 (1995).
[5] L.D. Macks, S.A. Brown, R.G. Clark, R.P. Starrett, M.A. Reed, M.R. Deshpande, C.J.L. Fernando, and W.R. Frensley, Phys. Rev. B **54**, 4857 (1996).
[6] S. Maimon, S.E. Schacham, G. Bahir, E. Finkman, and D. Ritter, Phys. Rev. B **54**, 5696 (1996).
[7] T. Kumar, M. Cahay, and K. Roenker, Phys. Rev. B **56**, 4836 (1997).
[8] A. Reklaitis and L. Reggiani, Phys. Rev. B **60**, 11 683 (1999).
[9] P.A. Lebwohl and P.J. Price, Appl. Phys. Lett. **19**, 530 (1971).
[10] E. Kollberg and A. Rydberg, Electron. Lett. **25**, 1696 (1989).
[11] A. Rydberg, H. Gronqvist, and E. Kollberg, IEEE Electron Device Lett. **11**, 373 (1990).
[12] J.P. Sun, R.K. Mains, W.L. Chen, J.R. East, and G.I. Haddad, J. Appl. Phys. **72**, 2340 (1992).
[13] Y. Fu, J. Stake, L. Dillner, M. Willander, and E.L. Kollberg, J. Appl. Phys. **82**, 5568 (1997).
[14] V.K. Reddy and D.P. Neikirk, Electron. Lett. **29**, 464 (1993).
[15] A.P. Long, P.H. Beton, and M.J. Kelly, J. Appl. Phys. **62**, 1842 (1987).
[16] S. Adachi, J. Appl. Phys. **58**, R1 (1985).
[17] T. Inata, S. Muto, Y. Nakata, S. Sasa, T. Fujii, and S. Hiyamizu, Jpn. J. Appl. Phys. **26**, L1332 (1987).
[18] I. Mehdi and G. Haddad, J. Appl. Phys. **67**, 2643 (1990).
[19] A. Reklaitis, J. Appl. Phys. **80**, 1242 (1996).
[20] H.C. Liu, Appl. Phys. Lett. **51**, 1019 (1987).
[21] M.V. Petrov, S.R. Parihar, and S.A. Lyon, Phys. Rev. B **54**, 13 868 (1996).
[22] J.J. Finley, R.J. Teissier, M.S. Skolnick, J.W. Cockburn, R. Grey, G. Hill, and M.A. Pate, Phys. Rev. B **54**, R5251 (1996).
[23] R. Teissier, J.J. Finley, M.S. Skolnick, J.W. Cockburn, J.-L. Pelouard, R. Grey, G. Hill, M.A. Pate, and R. Planel, Phys. Rev. B **54**, R8329 (1996).
[24] T. Osotchan, V.W.L. Chin, and T.L. Tansley, Phys. Rev. B **54**, 2059 (1996).
[25] M. Hosoda, K. Tominaga, N. Ohtani, K. Kuroyanagi, N. Egami, H. Mimura, K. Kawashima, and K. Fujiwara, Appl. Phys. Lett. **71**, 2827 (1997).
[26] J.B. Xia, Phys. Rev. B **41**, 3117 (1990).
[27] D. Junevičius and A. Reklaitis, Electron. Lett. **24**, 1307 (1988).
[28] A. Reklaitis, Phys. Lett. A **88**, 367 (1982).